CALCULATION OF A SEPARATED TURBULENT BOUNDARY LAYER

Barrett Baldwin
Ames Research Center

Ching Mao Hung
DCW Industries and Ames Research Center

SUMMARY

The properties of a Navier-Stokes solution of a shock-separated turbulent flow over a flat wall are investigated. Refinements of an algebraic relaxation turbulence model previously shown to be of value for the simulation of separated flows are presented. A simplified analysis applicable near an adiabatic wall is developed and used to help verify the accuracy of the numerical solution. Features of the time-dependent response of a turbulent boundary layer to shock impingement are presented.

INTRODUCTION

Computers now available are capable of practical calculations of complex flow fields, including separated turbulent boundary layers. However, as discussed in reference 1, development of adequate turbulence models is a pacing item that impedes progress toward that goal. Recent improvements in numerical methods, such as those described in reference 2, have made it feasible to test a variety of modifications of existing turbulence models (see, e.g., references 3-5 and the more comprehensive reference lists therein). For engineering purposes, it would be practical to use simplified models calibrated from experiments conducted at nearby flow conditions. The shortage of experimental information on separated flows prevents calibration with precision at this time. Nevertheless, it seems worthwhile to proceed with the development of computer codes for complex flows based on simplified turbulence models that can be adjusted to accommodate the existing experiments. With presently available information, it may be possible to accomplish this for high Reynolds number flows at Mach numbers up to 3 using the boundary-layer approximation for viscous and Reynolds stress terms in the layers near solid surfaces. More complicated procedures can be incorporated when they are justified or can be used to aid in the calibration of the simplified models.

In reference 5, it was shown that an inner layer algebraic eddy viscosity model used by Clauser (ref. 6) provides better agreement with two separated flow experiments than more conventional models. In this paper, the properties of a Navier-Stokes solution of a shock-separated flow based on a variation of that

model are investigated. A simplified analysis applicable near an adiabatic wall is presented. Favorable comparisons of results from this analysis with the Navier-Stokes solution show that the boundary-layer approximation is valid near the wall for this case and that the Navier-Stokes solution is accurate. As an example of the type of information that can result from such numerical solutions, features of the time-dependent response of a boundary layer to impingement of a shock wave are presented.

SYMBOLS

A	constant (eq. (22))
B	constant (eq. (23))
B_{F3}	constant in turbulence model (eq. (6))
C	constant (eq. (17))
C_p	specific heat at constant pressure
$f_1(y+)$	universal function (eq. (18))
$f_2(y+)$	universal function (eq. (19))
k	Karman constant (0.4)
K	Clauser constant (0.016)
p	pressure, N/m^2 (lb/ft^2)
P_{RT}	turbulent Prandtl number (0.9)
S_1, S_2	constants in Sutherland viscosity law (eq. (20))
T	temperature, K (°R)
u	velocity in x-direction, m/sec (ft/sec)
$u_{\tau 2}$	friction velocity (eq. (4)), m/sec (ft/sec)
$u_{\tau 3}$	friction velocity (eq. (5)), m/sec (ft/sec)
V	constant in Van Driest damping factor (eq. (8))
V_F	Van Driest damping factor (eq. (8))
x,y	Cartesian coordinates, m (ft)
y^+	law of the wall variable (eq. (9))

δ boundary-layer thickness, m (ft)

δ^* kinematic displacement thickness (eq. (10)), m (ft)

λ relaxation parameter (eq. (5))

μ molecular coefficient of viscosity, kg/m-sec (slugs/ft-sec)

μ_t turbulent eddy viscosity coefficient (eqs. (1),(2)) kg/m-sec (slugs/ft-sec)

ρ gas density, kg/m^3 ($slugs/ft^3$)

τ shear stress (eq. (11)), N/m^2 (lb/ft^2)

Subscripts:

0 initial profile at station ahead of interaction

2 value of y at which $u_{\tau 2}$ is evaluated (eqs. (3),(4))

3 value of y at which $u_{\tau 3eq}$ is evaluated (eq. (6))

i position of inviscid shock impingement on wall

max maximum velocity in profile

w value at wall

METHOD

Numerical Method for Navier-Stokes Solutions

The basic numerical method used in this investigation is described in reference 7. Recently, MacCormack has improved the method such that the calculations require an order of magnitude less computation time than formerly (see ref. 2). The compressible Navier-Stokes equations to be solved are also listed in reference 7.

Experiment Used for Comparison

The experimental flow field (ref. 8) is depicted in figure 1. A shock wave generated by a plate set at 13° to the free stream impinges on the boundary layer on the upper wind tunnel wall. A separation bubble containing reversed flow forms and extends upstream of the inviscid shock impingement point. A pattern containing induced and reflected shocks forms. The free-stream Mach number is 3 and the Reynolds number based on initial boundary-layer thickness ahead of the interaction is 10^6.

Turbulence Model

The two-layer algebraic eddy viscosity model used in the present calculations is defined by the following equations:

$$(\mu_t)_{inner} = \left\{ \begin{array}{ll} \rho_2 \frac{\mu}{\mu_2} kyu_{\tau 3} V_F^2 & , \quad (y \leq y_2) \\ \rho kyu_{\tau 3} V_F^2 & , \quad (y > y_2) \end{array} \right\} ; \quad k = 0.4 \tag{1}$$

$$(\mu_t)_{outer} = K\rho u_{max} \delta^* \quad , \quad K = 0.0168 \tag{2}$$

where ρ_2 and μ_2 are evaluated at $y = y_2$ with y_2 determined from the relations

$$\tilde{y}_2^+ = \left(\frac{\rho u_{\tau 2} y}{\mu} \right)_{y=y_2} = 100 \tag{3}$$

$$u_{\tau 2} = \left(ky \frac{\partial u}{\partial y} \right)_{y=y_2} \tag{4}$$

The quantity $u_{\tau 3}$ is determined from the relaxation formula

$$\frac{du_{\tau 3}}{dx} = \frac{u_{\tau 3 eq} - u_{\tau 3}}{\lambda \delta_0} \quad , \quad \lambda = 5 \tag{5}$$

where

$$u_{\tau 3 eq} = B_{F3} \left(ky \frac{\partial u}{\partial y} \right)_{y=y_3} \quad , \quad B_{F3} = 1.18 \tag{6}$$

with y_3 determined from the relation

$$\tilde{y}_3^+ = \left(\frac{\rho ky \frac{\partial u}{\partial y} y}{\mu} \right)_{y=y_3} = 2000 \tag{7}$$

The quantity V_F is the Van Driest damping factor

$$V_F = 1 - \exp(-y^+/V) \quad , \quad V = 18 \tag{8}$$

where

$$y^+ = \frac{\rho_2 u_{\tau 3} y}{\mu_2} \tag{9}$$

The transition from the inner to the outer formula takes place at the minimum value of y at which $(\mu_t)_{inner} = (\mu_t)_{outer}$. The kinematic displacement thickness δ^* is given by

$$\delta^* = \int_0^{\delta} \left(1 - \frac{u}{u_{max}}\right) dy \tag{10}$$

The foregoing model differs from that developed in reference 5 in several respects. Replacement of ρ with $\rho_2\mu/\mu_2$ at $y < y_2$ in equation (1) has the effect of removing the dependence of μ_t/μ on variations of temperature and density in the viscous sublayer. Although future experimental data may show such a dependence, it seems preferable at this time to make μ_t/μ dependent on y^+ alone, and thus to maintain a close correspondence with incompressible flows. Additionally, the factor B_{F_3} in equation (6) allows a close correspondence of the present inner layer Clauser model with more conventional models for flows with zero pressure gradient. Finally, use of y^+ as defined in equation (9) in the Van Driest damping factor instead of the definition used in reference 5 requires rescaling of V to $V = 18$.

Simplified Analysis Applicable Near an Adiabatic Wall

The following approximate relationships, obtained from the compressible Navier-Stokes equations, are useful for checking the adequacy of the mesh used for the numerical solution. They may also be useful for deducing values of parameters in the turbulence model from experimental data obtained from separated and attached boundary-layer flows with pressure gradients. Upon neglecting the convection and inertia terms, the steady-state x-momentum and energy equations can be approximated by

$$\tau = (\mu + \mu_t)\frac{du}{dy} = \tau_2 + (y - y_2)\frac{dp}{dx} \tag{11}$$

$$\frac{C_p T}{P_{RT}} + \frac{1}{2}u^2 = \frac{C_p T_2}{P_{RT}} + \frac{1}{2}u_2^2 \quad \text{(adiabatic wall)} \tag{12}$$

Replacement of the y-momentum equation with $\partial p/\partial y = 0$ and use of the equation of state for a perfect gas yields

$$\frac{\rho}{\rho_2} = \frac{T_2}{T} \tag{13}$$

With the definition

$$du^+ = \begin{cases} \dfrac{\mu}{\mu_2}\, du/C, & (y \leq y_2) \\ \dfrac{\rho}{\rho_2}\, du/C, & (y > y_2) \end{cases} \tag{14}$$

and substitution of the foregoing inner-layer eddy viscosity model into equation (11), the following expression for u^+ can be derived:

$$u^+ = (1 - p^+) f_1(y^+) + \frac{p^+}{y_2^+} f_2(y^+) \tag{15}$$

where

$$p^+ = y_2 \frac{dp/dx}{\tau_2} = 1 - \frac{\tau_w}{\tau_2} \tag{16}$$

$$C = u_{\tau 2}\left[\frac{1}{k y_2^+} + V_F^2(y_2^+)\right] \approx u_{\tau 2} \tag{17}$$

$$f_1(y^+) = \int_0^{y^+} \frac{dy^+}{1 + k y^+ V_F^2(y^+)} \approx 5.5 + \frac{1}{k} \ln(y^+) \tag{18}$$

$$f_2(y^+) = \int_0^{y^+} \frac{y^+ dy^+}{1 + k y^+ V_F^2(y^+)} \approx \frac{1}{k} y^+ \tag{19}$$

The approximations for f_1 and f_2 on the right apply at $y^+ \gtrsim 60$ where $V_F \approx 1$.

To obtain the relation between u^+ and u, we use the Sutherland viscosity law in the form

$$\mu(T) = \frac{S_1 T^{3/2}}{S_2 + T} \tag{20}$$

Linearization of the Sutherland relation and substitution of equations (12) and (13) into (14) leads to

$$u^+ = \begin{cases} \dfrac{\mu_w}{\mu_2}\left(1 - \dfrac{1}{3} AB^2 u^2\right) \dfrac{u}{C} & (u \leq u_2) \\ u_2^+ + \dfrac{BC_p T_2}{C P_{RT}} \ln\left[\dfrac{(1 + Bu)(1 - Bu_2)}{(1 - Bu)(1 + Bu_2)}\right] & (u > u_2) \end{cases} \tag{21}$$

where

$$A = \frac{2 + 3S_2/T_w}{1 + S_2/T_w} \tag{22}$$

$$B = \left(\frac{2C_p T_2}{P_{RT}} + u_2^2\right)^{-1/2} \tag{23}$$

RESULTS AND DISCUSSION

A time-dependent solution of the compressible Navier-Stokes equations based on the foregoing eddy viscosity model has been carried out. The initial flow field is uniform in the x-direction with a boundary-layer profile corresponding to an upstream station in the experiment of reference 8. At the lower boundary of the computational field, boundary conditions are imposed corresponding to the shock wave in the experiment (see fig. 1). During the calculation, the shock wave grows toward the upper nozzle wall. Eventually, a steady state is reached corresponding to the conditions at which experimental measurements were made. As an illustration of the type of information that can result from such calculations, features of the time-dependent response of the boundary layer to growth of the incident, induced, and reflected shock pattern will be presented. However, the simplified analysis in the preceding section will first be used to check the adequacy of the computational mesh.

The steady-state Navier-Stokes solution was used to compute dimensionless profiles of u^+ versus y^+ according to equations (9) and (21). Three such profiles are contained in figure 2. The circles represent the Navier-Stokes solution and are at the computational mesh points. The dashed lines are obtained from the simplified analysis (eq. 15)), using values of p^+ and y_2^+ evaluated from the Navier-Stokes solution according to equations (3), (4), (9) and (16). The upper two profiles are at stations aft of reattachment where relatively small pressure gradients are present. The bottom profile is in the region of constant pressure ahead of the separated region, which extends from $-2.6 \lesssim (x - x_1/\delta_0) \lesssim 0.5$. The close correspondence between the approximate and numerical solutions leads to two conclusions: (1) Use of the boundary-layer approximation with additional neglect of convection and inertia terms is a valid approximation near the wall for small pressure gradients; and (2) the computational mesh used for the Navier-Stokes solution provides adequate resolution. However, are the same conclusions valid at stations where strong pressure gradients exist?

Profiles near separation and in the middle of the reversed flow bubble are shown in figure 3. Again the Navier-Stokes solution is represented by symbols and the simplified boundary-layer approximation by dashed lines. Near separation, the approximate results are invalid for values of y^+ greater than about 300 because of neglect of the convection and inertia terms. In the middle of the separation (lower curve), the simplified analysis retains validity to large values of y^+. The resolution of the Navier-Stokes solution is again shown to be adequate. Profiles near reattachment are shown in figure 4. The two solutions agree closely over a large range of y^+ in this region.

With confidence in the resolution of the Navier-Stokes solution established, it is of interest to observe the time-dependent response of the boundary layer to shock impingement. Figure 5 contains plots of wall pressure distribution at a series of time intervals after the start of the calculation. Shortly after the shock reaches the boundary layer and a reflected shock has formed, the wall pressure rise is steep and extends about one boundary-layer thickness upstream of the inviscid shock impingement point, which occurs at 0 on the

abscissa scale. During succeeding time intervals, the pressure gradient decreases and the pressure rise moves upstream. Eventually, a steady state is reached in which the initial pressure rise occurs about three boundary-layer thicknesses ahead of the inviscid shock impingement point. The plot at the top includes the corresponding experimental steady-state pressure distribution from reference 8 for comparison.

Figure 6 contains plots of the skin-friction distributions after the same series of time intervals. In the plot at the top, the calculations are in close agreement with a Preston tube measurement of the initial skin-friction coefficient C_f and oil-flow observations of separation and reattachment points (ref. 8). Skin-friction measurements were not made at other stations in this experiment.

REFERENCES

1. Chapman, D. R.; Mark, H.; and Pirtle, M. W.: Computers vs Wind Tunnels for Aerodynamic Flow Simulation. Astronautics and Aeronautics, vol. 13, no. 4, April 1975, pp. 22-30.

2. MacCormack, R. W.: A Rapid Solver for Hyperbolic Systems of Equations. Paper presented at 5th International Conference on Numerical Methods in Fluid Dynamics, The Netherlands, June 28 to July 3, 1976.

3. Hung, C. M. and MacCormack, R. W.: Numerical Simulation of Supersonic and Hypersonic Turbulent Compression Corner Flows Using Relaxation Models. AIAA Paper 76 — presented at AIAA 9th Fluid Dynamics Conference in San Diego, July 14-16, 1976.

4. Horstman, C. C.: A Turbulence Model for Nonequilibrium Adverse Pressure Gradient Flows. AIAA Paper 76-412, presented at AIAA 9th Fluid and Plasma Dynamics Conference in San Diego, July 14-16, 1976.

5. Baldwin, B. S. and MacCormack, R. W.: Modifications of the Law of the Wall and Algebraic Turbulence Modeling for Separated Boundary Layers. AIAA Paper 76-350, presented at AIAA 9th Fluid and Plasma Dynamics Conference in San Diego, July 14-16, 1976.

6. Clauser, F.: On Turbulent Flow Near a Wall. Jour. Aero. Sci., vol. 23, no. 11, 1956, pp. 1007-1011.

7. MacCormack, R. W. and Baldwin, B. S.: A Numerical Method for Solving the Navier-Stokes Equations with Application to Shock-Boundary Layer Interactions. AIAA Paper 76-1, presented at AIAA 13th Aerospace Sciences Meeting in Pasadena, Jan. 20-22, 1975.

8. Reda, D. C. and Murphy, J. D.: Shock Wave Turbulent Boundary Layer Interaction in Rectangular Channels, Part II: The Influence of Sidewall Boundary Layers on Incipient Separation and Scale of Interaction. AIAA Paper 73-234 presented at AIAA 11th Aerospace Sciences Meeting in Washington, D. C., Jan. 10-12, 1973.

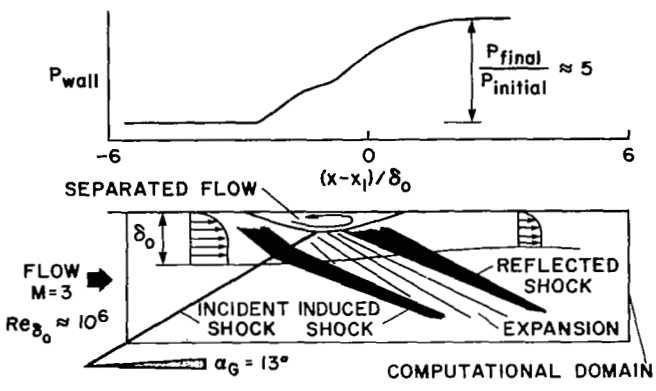

Figure 1.- Experimental flow field.

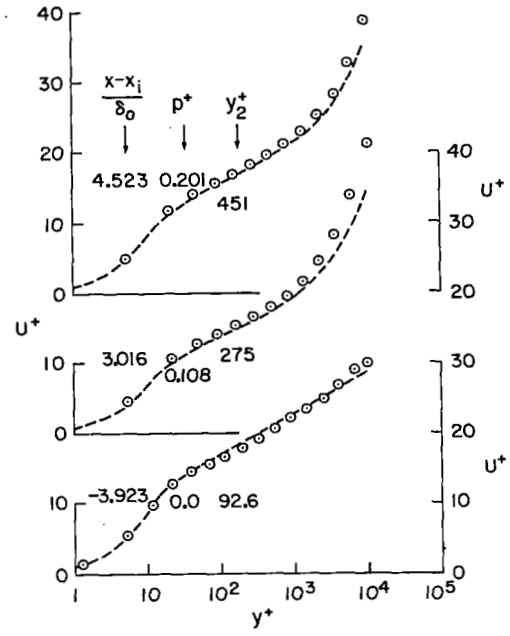

Figure 2.- Attached velocity profiles.

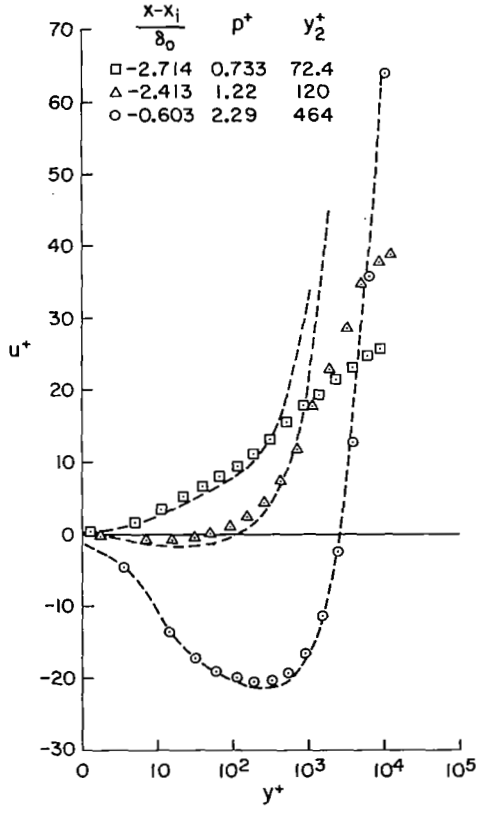

Figure 3.- Velocity profiles near separation.

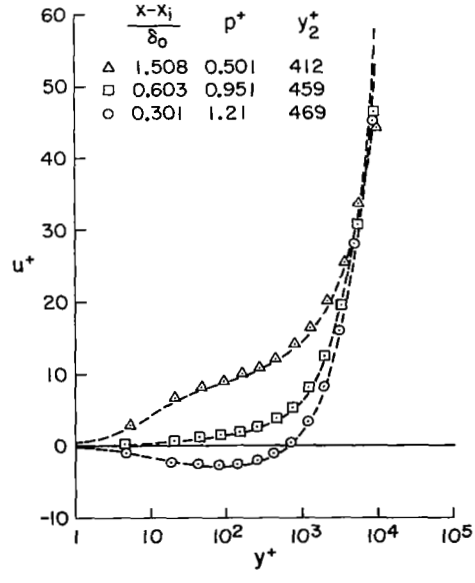

Figure 4.- Velocity profiles near reattachment.

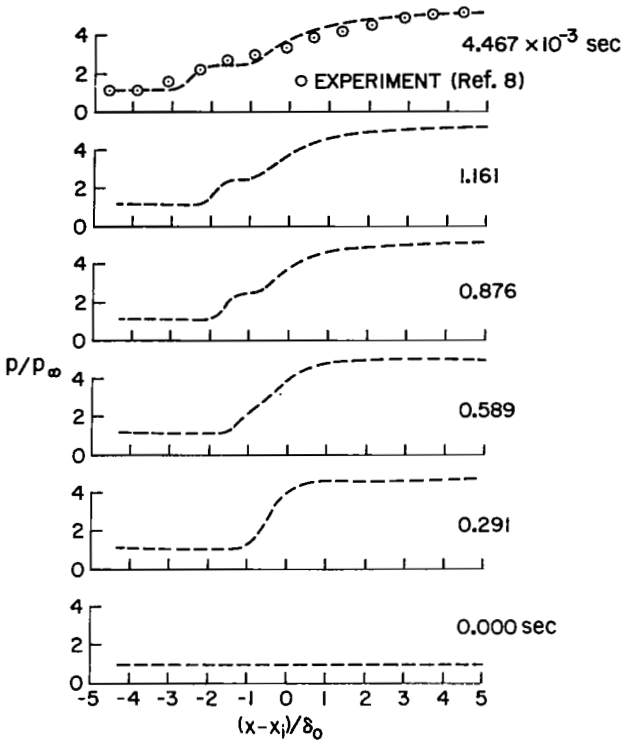

Figure 5.- Response of wall-pressure distribution.

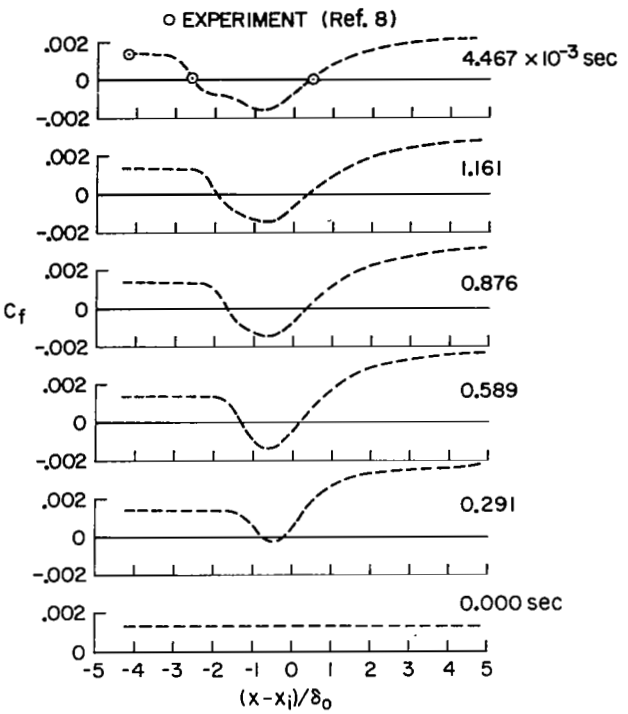

Figure 6.- Response of skin-friction distribution.